Boletín Geológico

SERVICIO GEOLÓGICO COLOMBIANO

Boletín Geológico, 49(1), 7-27, 2022

https://doi.org/10.32685/0120-1425/bol.geol.49.1.2022.571

Received: March 12, 2021

Revision received: August 24, 2021

Accepted: September 15, 2021

Published online: December 10, 2021

Research article

Petrographic, chemical and geochronological characteristics of the Onzaga Metarhyolite and its correlation with Ordovician magmatic events in the northern Andes, Colombia

Características petrográficas, químicas y geocronológicas de la Metariolita de Onzaga y su correlación con eventos magmáticos ordovícicos en los Andes del norte, Colombia

Gabriel **Rodríguez García**[1]

1 Servicio Geológico Colombiano, Special Geological Studies Group, Medellín, Colombia.
Corresponding author: grodriguez@sgc.gov.co

Abstract

The macroscopic, microscopic, and chemical characteristics as well as crystallization age of the Onzaga Metarhyolite unit are described. The spatiotemporal relationships among the magmatic events that occurred during the Ordovician in the Santander, La Floresta and Quetame massifs and in the Mérida Mountain range are analyzed. Additionally, a correlation is made with plutonic bodies that have crystallization ages within this same period of time.

The Onzaga Metarhyolite outcrops in the Santander massif in the surroundings of the municipality of Onzaga-Santander, with an approximate area of 155 km^2; it is composed of metavolcanic rocks that are chemically classified as rhyolites, which were affected by metamorphism in green schist facies to low amphibolite. The metarhyolites are composed of quartz porphyroclasts, plagioclase and alkali feldspar, and some retain the textures and relict forms of the phenocrysts, which are found within a microcrystalline matrix, with local development of quartz mosaics and oriented sheets of white mica and biotite.

The rocks of the Onzaga Metarhyolite have high contents of SiO_2 (76.9% to 79.3%), K_2O (4.03% to 5.66%) and Al_2O_3 (11.5% to 14.3%) and low contents of Fe_2O_3, TiO_2, CaO, MnO and MgO. The rocks have alkali values ($Na_2O + K_2O$) between 5.3% and 7.9% and $K_2O/Na_2O > 2$. They are classified within the calc-alkaline rocks high in K, peraluminous, and related to magmas that generate type S granites. In the multielement diagrams, Nb has a weak negative anomaly, as does Zr, while the negative anomalies of Ti and Sr are pronounced. Higher values of lithophilic elements of high ionic radius (LILE) Cs, Ba and Th indicate a continental crust

Citation: Rodríguez, G. (2022). Petrographic, chemical and geochronological characteristics of the Onzaga Metarhyolite and its correlation with Ordovician magmatic events in the northern Andes, Colombia. *Boletín Geológico, 49*(1), 7-27. https://doi.org/10.32685/0120-1425/bol.geol.49.1.2022.571

affinity. The Eu/Eu * values are low, between 0.12 and 0.74. The normalized values of $(La/Yb)_N$ vary between 4 and 24.4, $(La/Sm)_N$ varies between 2.2 and 2.5, and $(Eu/Yb)_N$ varies between 0.2 and 2.1.

Two samples of Onzaga Metarhyolite were analyzed by the LA-ICP–MS U-Pb method in zircon. The results analysis indicates a crystallization age that varies between 450.9 ± 2.5 Ma and 449.9 ± 5.9 Ma, with a second population between 475.9 ± 5.4 Ma and 469.8 ± 4.0; these ages are interpreted as magmatic zircons inherited from a lower to middle Ordovician igneous event. The zircons have xenocrysts and inherited nuclei of 555 ± 11 Ma and 565.7 ± 9 Ma and populations of 617 ± 16 Ma (n = 3) and 644.5 ± 6.5 (n = 3), respectively, and three inheritances between 1071 ± 48 Ma and 1171 ± 37 Ma.

Keywords: U-Pb geochronology, Santander Massif, volcanism, Ordovician.

Resumen

Se describen las características macroscópicas, microscópicas, químicas y la edad de cristalización de la unidad. Se analiza la relación espacio-temporal con los eventos magmáticos que ocurrieron durante el Ordovícico en los macizos de Santander, La Floresta y Quetame, y en la cordillera de Mérida. Adicionalmente, se hace una correlación con cuerpos plutónicos que tienen edades de cristalización en este mismo periodo de tiempo.

La Metariolita de Onzaga aflora en el macizo de Santander, en los alrededores del municipio de Onzaga-Santander, con un área aproximada de 155 km^2; está constituida por rocas metavolcánicas que clasifican químicamente como riolitas, las cuales fueron afectadas por metamorfismo en facies esquisto verde a probablemente anfibolita baja. Las metariolitas están constituidas por porfidoclastos de cuarzo, plagioclasa y feldespato alcalino, algunos conservan las texturas y formas relictas de los fenocristales; estos se encuentran dentro de una matriz microcristalina, con desarrollo local de mosaicos de cuarzo y láminas orientadas de mica blanca y biotita.

Las rocas de la Metariolita de Onzaga presentan altos contenidos de SiO_2 (76,9 % a 79,3 %), K_2O (4,03 % a 5,66 %) y Al_2O_3 (11,5 % a 14,3 %), y bajos contenidos de Fe_2O_3, TiO_2, CaO, MnO y MgO. Tienen valores de álcalis ($Na_2O + K_2O$) entre 5,3 % y 7,9 % y $K_2O/Na_2O > 2$. Se clasifican dentro de las rocas calcoalcalinas altas en K, peraluminosas, afines a los magmas que generan granitos Tipo S. En los diagramas multielementales el Nb presenta una débil anomalía negativa, al igual que el Zr, mientras las anomalías negativas de Ti y Sr son pronunciadas. Los mayores valores de los elementos litófilos de alto radio iónico (LILE) Cs, Ba y Th indican una afinidad de corteza continental. Los valores Eu/Eu* son bajos entre 0,12 y 0,74. Los valores normalizados de $(La/Yb)_N$ varían entre 4 y 24,4; $(La/Sm)_N$ varían entre 2,2 y 2,5, y $(Eu/Yb)_N$ entre 0,2 y 2,1.

Se analizaron dos muestras de la Metariolita de Onzaga por el método LA-ICP-MS U-Pb en circón. El análisis de los resultados indica una edad de cristalización que varía entre 450,9 ± 2,5 Ma y 449,9 ± 5,9 Ma, con una segunda población entre 475,9 ± 5,4 Ma y 469,8 ± 4,0; estas edades se interpretan como circones magmáticos heredados de un evento ígneo Ordovícico inferior a medio. Los circones presentan xenocristales y núcleos heredados de 555 ± 11 Ma y 565,7 ± 9 Ma, poblaciones de 617 ± 16 Ma (n = 3) y 644,5 ± 6,5 (n = 3) y tres herencias entre 1071 ± 48 Ma y 1171 ± 37 Ma.

Palabras clave: geocronología U-Pb, Macizo de Santander, vulcanismo, Ordovícico.

1. Introduction

The first descriptions of this unit were made by Vargas et al. (1976, 1981), who named it Riolitas de Onzaga. The rhyolitic body outcrops in the surroundings of the municipality of Onzaga-Santander and extends south toward the Páramo de Canutos. The unit occupies an area of approximately 155 km^2 and is present in a strip with an average width of 4.5 km and an average length of 35 km. The directional tendency is mainly N-S, and in its southwestern portion, it presents a NE-SW directional tendency. The Onzaga Metarhyolite has been considered an effusive product of the granitic bodies of Mogotes and Santa Rosita of Jurassic-Triassic age (Vargas et al., 1981).

This article presents new data from petrography (7 analyses), total rock chemistry (4 analyses) and U-Pb geochronology in zircon (2 analyses) for the metavolcanic rocks of the unit called Onzaga Metarhyolite. The mineralogy and characteristics of the metamorphism that affect the unit are described. The name On-

zaga Metarhyolite is proposed, considering the metamorphism on tax. Crystallization ages of the Upper Ordovician were obtained, and these ages relate the unit to magmatic events of the Paleozoic in the Santander Massif and subsequently to the main event of the Famatinian orogeny of *ca.* 470 Ma.

2. Regional geological framework

The Santander Massif (MS) is located in the Eastern Cordillera of Colombia and is part of a regional block limited by the Santa Marta-Bucaramanga faults on the western side, the Oca fault on the northern side and the Boconó fault on the side (Cediel et al., 2003; Mantilla et al., 2013; van der Lelij et al., 2016).

The MS is formed by a metamorphic basement represented by the Bucaramanga gneiss, the Silgará Formation and granitic orthogneisses (Ward et al., 1973). The Bucaramanga gneiss consists of sillimanite-cordierite gneiss with garnet, amphibolic gneiss, feldspathic quartz granofels and amphibolites with migmatitic structures (Ward et al., 1973), with metamorphism ages of approximately 477 Ma (van der Lelij, 2013, van der Lelij et al., 2016). Overlying the Bucaramanga gneiss is the Silgará Formation (Ward et al., 1973), called the Silgará schist by Mantilla et al. (2016), composed of schists, phyllites, meta-lodolites, meta-sandstones and marbles of Paleozoic age (Clavijo et al., 2008; Mantilla et al., 2012; Ordóñez-Cardona et al., 2006; Ríos et al., 2003; van der Lelij et al., 2016; Zuluaga et al., 2017). Ordovician deformed granitoids ("Unit of orthogneisses", according to Ward et al., 1973) intrude the Bucaramanga gneiss and the Silgará Formation. The three units mentioned above record a common event of Ordovician metamorphism that affected the entire basement of the MS (Mantilla et al., 2012, 2013; Restrepo-Pace et al., 1997; van der Lelij et al., 2016; Zuluaga et al., 2017).

In the MS, there is a record of Paleozoic and Mesozoic magmatism. The first is represented by orthogneiss, plutons and volcanics, which originated from magmatic events before and after the Famatinian orogeny, and most of them are associated with a continental arc environment. The igneous bodies are Ordovician, Silurian, Lower Devonian and Carboniferous; among them are orthogneiss from Berlin and monzogranite from Cáchira (Leal-Mejía, 2011; Mantilla et al., 2012; Restrepo-Pace, 1995; Ulloa and Rodríguez, 1982; van der Lelij, 2013; van der Lelij et al., 2016, Zapata et al., 2017). Mesozoic magmatism is mainly from the late Triassic to the Upper Jurassic and includes batholiths and stocks located in the core and along the western edge of the MS (Rodríguez et al., 2017, 2020a). Small bodies of Albian-Cenomanian dikes intrude the Triassic-Jurassic granitoids (Correa-Martínez et al., 2017).

The Onzaga Metarhyolite is limited to the west, with metasedimentary rocks of the Silgará Formation and granitic intrusion by the Canutos Stock. To the east, the unit is in contact with Cretaceous and Devonian sediments. The Silgará Formation is crossed by dikes and rhyolitic silos that correlate with the Onzaga metarhyolite, which presents xenoliths of metamorphic rocks. To the south, contact with the Canutos Stock granite was described as likely transitional (Figure 1).

3. Methods

In this research, regional sampling was performed to cover the entire MS, including the Onzaga Metarhyolite on the eastern side of the massif.

3.1. Petrography

Two petrographic analyses were compiled in cartography projects by the Colombian Geological Survey (previously Ingeominas). Five new thin sections were elaborated in Bogotá, which were analyzed in the Petrography Laboratory of the Colombian Geological Service in the Medellín region using Leitz and Olympus petrographic microscopes for the analysis; the classification was made from 300 counting points using Streckeisen triangles (1978) and following the recommendations of the Subcommittee on Metamorphic Rocks (Schmid et al., 2007).

3.2. Chemical analysis of total rock

Four chemical analyses of total rock were carried out in the Analytical Geochemistry Laboratory of the Colombian Geological Service, Bogotá. The major oxides and minor elements were analyzed with a Panalytical AXIOS Mineral X-ray fluorescence spectrometer; the former were quantified from samples fused with lithium metaborate and tetraborate, while the latter were quantified in pressed samples. For the analysis of trace elements, a mass spectrometer with inductively coupled plasma ICP–MS, Perkin Elmer NEXION, was used.

Petrographic and geochemical diagrams were obtained using the software GCDkit by Janoušek et al. (2006).

3.3. Geochronology

Two samples of metarhyolites were dated by the U-Pb method using laser ablation, together with inductive plasma-coupled mass spectrometry (LA-ICP-MS) in zircon. The zircons were concen-

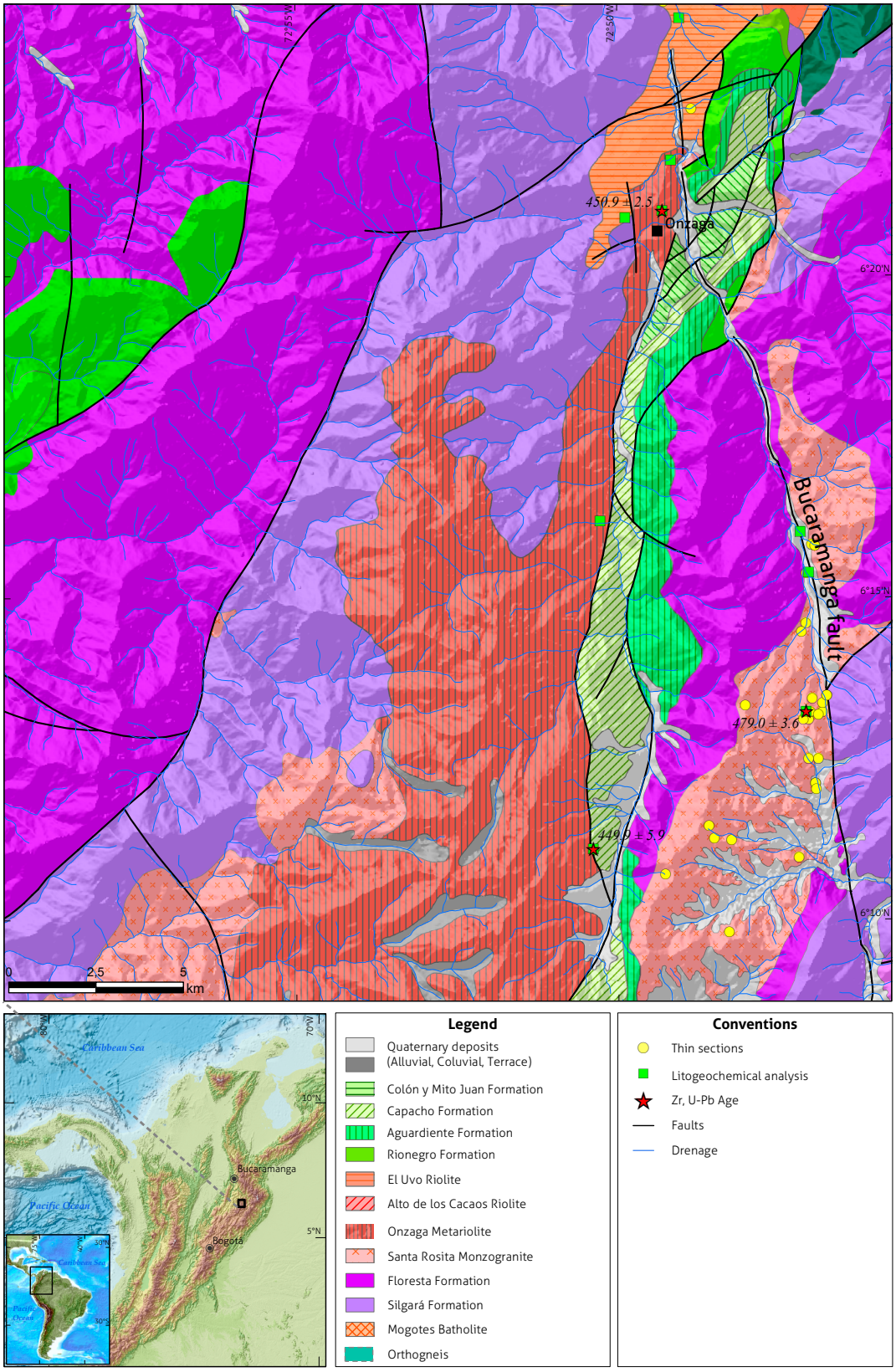

Figure 1. Geological map of the Onzaga Metarhyolite
Distribution of petrography, geochronology and total rock chemistry samples. Source: Vargas et al. (1987), Ulloa et al. (1998), and this work.

trated in the Chemical Laboratory of the Colombian Geological Service, Medellín, using hydrodynamic and magnetic separation. Then, they were manually selected with an Olympus binocular magnifying glass in the Petrography Laboratory at the Medellín headquarters. Cathodoluminescence (LC) images were acquired from the zircon grain assemblies by means of luminoscopes.

A sample was analyzed in the Laboratory of Isotopic Studies (LEI) at the Geosciences Center of the National Autonomous University of Mexico (UNAM), Juriquilla campus, using a Thermo X series QICPMS coupled to a Resonetics, Excimer Laser Workstation Resolution M050; the procedures and equipment are described in Solari et al. (2010). The analyzed points were 23 μm; the propagated 2-sigma uncertainties were achieved according to Paton et al. (2010). The $^{207}Pb/^{206}Pb$ ratios, ages and errors were calculated according to Petrus and Kamber (2012). The concentrations of U and Th were calculated using an external standard zircon according to Paton et al. (2010).

The second sample was analyzed in the laboratories of the Colombian Geological Survey. The rock samples were crushed, pulverized and sieved following the separation procedures of Castaño et al. (2018) and analyzed by LA-ICP-MS according to the procedures described in Peña et al. (2018). The zircons were concentrated in the Chemical Laboratory of the Colombian Geological Service, Medellín, using hydrodynamic and magnetic separation and by batting for some samples in the field. Then, they were manually selected with an Olympus binocular magnifying glass in the Petrography Laboratory of the Medellín headquarters. Cathodoluminescence (LC) images were acquired from the zircon grain assemblies.

The analyses were performed in photon machine ablation equipment with a 193-nm excimer laser coupled to an Element 2-type mass spectrometer. The isotopes used for manual integration are ^{238}U, ^{206}Pb and ^{204}Pb. As reference standards, Plešovice (Sláma et al., 2008), FC-1 (Coyner et al., 2004), Zircón 91500 (Wiedenbeck et al., 1995, 2004) and Mount Dromedary (Renne et al., 1998) were used. The analyzed points in the zircons were 20 microns in diameter. Plešovice (Sláma et al., 2008), 91500 (Wiedenbeck et al., 2004) and mount dromedary (Renne et al., 1998) were used as reference standards. Data reduction was performed using the Iolitev2.5® program in IGORPro6.3.6.4® (Paton et al., 2010; Hellstrom et al., 2008). The correction for common lead was performed according to the evolution model from Stacey and Kramers (1975). The final results correspond to the mean of the data obtained after applying data discrimination to two standard deviations.

4. Results

4.1. Macroscopic and microscopic description

Figure 2c shows the Streckeisen diagram (1978) and the classification based on the phenocrysts of the rock protolith. Table 1 summarizes the petrographic results.

The rocks presented as banded, and the mineral orientation showed development of schistosity (Figure 2, a and b); the rocks are composed of metarhyolites, metadacites and metaquarzites of light pinkish brown to light greenish brown color, where quartz, plagioclase and feldspar porphyroclasts, (old phenocrysts) are recognized as alkaline in a pinkish-brown, aphanitic matrix. The porphyroclasts are 1 to 2.5 mm, with some rounded and others elongated in the manner of augens, and in some samples, they conserve the primary form of the volcanic rock (Figure 3). The rocks have relict textures of the porphyritic protolith. The matrix is lepidoblastic microgranoblastic, marked by sheets of muscovite and biotite together with polygonal microgranular mosaics of quartz and feldspars. It presents recrystallization of subgrains at the edges of feldspar and quartz porphyroclasts, as well as orientation of the micas, and relic textures are recognized in the old quartz phenocrysts, such as bays and paste drops in the matrix. It consists of porphyroclasts (phenocrysts) of plagioclase, feldspar and quartz, and in the matrix, it is composed of mosaics of quartz feldspars and thin sheets of white mica and biotite. Zircon, titanite, and opaque minerals are used as accessory minerals, and sericite from plagioclase and clay group minerals are used as alteration minerals.

Table 1. Modal composition of rocks of the Onzaga Metarhyolite

IGM	N field	X	And	Qtz	Pl	Fsp	Bt	Ms	Chl	Op	Zrn	Ttn	Matrix	Other	Petrographic classification
900893	GR-6733	1137174	1185242	13.5	9.4	11.5	2.1	15.0		TR	TR	TR	48.5		Meta Riolite
900913	JGB-467	1139441	1194628	22.7	16.3	5.7	TR		1	TR			53	1.3	Meta Dacite
900928	LMC-076	1138952	1194129	16	7	12		30		TR	TR		34	1	Meta Rhyolite
900968	TCR382	1139194	1195574	53.3	5	12		27		2	0.2	0.5			Meta Rhyolite
900992	JGB-483	1136986	1175847	6.1	3.4	5.4		TR		TR	TR		85.1		Meta Rhyolite
74832	OP-675	1121220	1164130	2.1	7	5.3	TR		TR	TR	TR		85.6	TR	Pheno quartzlatite

Qtz: quartz, Pl: plagioclase, Fsp: alkaline feldspar, Bt: biotite, Ms: muscovite (white mica), Chl: chlorite, Op: opaque minerals, Zrn: zircon, Ttn: titanite, TR: traces.

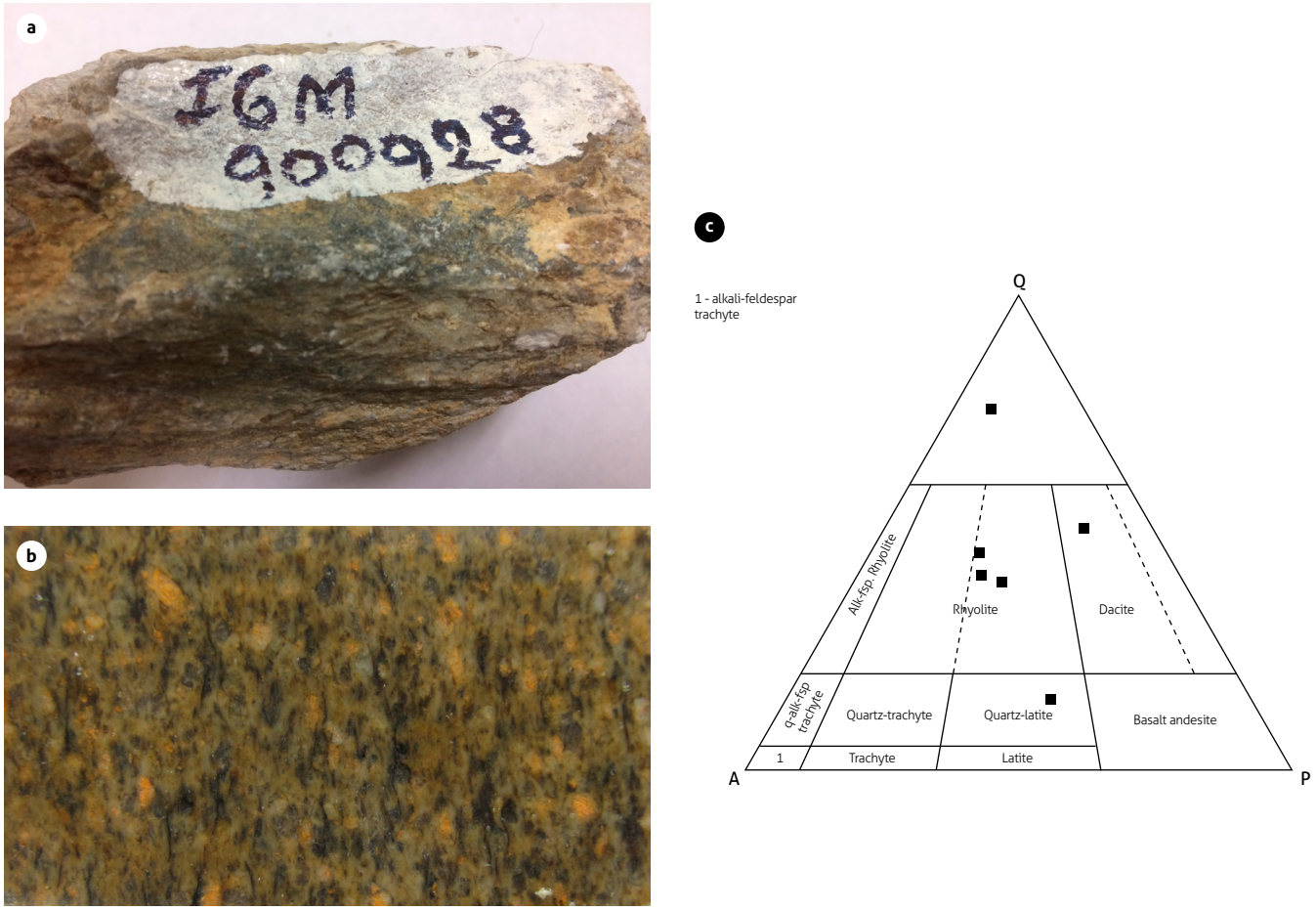

Figure 2. Macroscopic aspect of rocks of the Onzaga Metarhyolite and modal classification a) Sample LMC-076, b) Sample GR-6733 and c) Classification triangle (Streckeisen, 1978).

Quartz, plagioclase and alkaline feldspar appear as partially deformed porphyroclasts inherited from phenocrysts of the volcanic protolith (Figure 3, a, b, c and d). Porphyroclasts are oriented in the direction of the metamorphic foliation. The quartz crystals can retain the relict bipyramidal form, the corrosion bays of the matrix and the recrystallized paste droplets (Figure 3, a and b). They are of sizes between 0.5 mm and 2.5 mm, with marked wavelike extinctions, some with recrystallization to subgrains at the edges and along the lamellae that cross the phenocrysts. Plagioclase is albite to sodium oligoclase type, which occurs in euhedral to subhedral crystals of sizes between 0.75 mm and 2 mm; they are partially recrystallized subgrains at the edges with local patches inside the crystals and may or may not have twins of inherited albite and albite *Carlsbad* types (Figure 3, a and d). The alkaline feldspar presents poorly developed microcline twins and occasionally *Carlsbad*, and they are euhedral to subhedral (Figure 3, a, c and d), with wave extinctions; their specimens present recrystallization of microcrystalline mosaics at the edges and occasionally inside the crystals, have asymmetric pressure shadows caused by dynamic metamorphism, are powdered by biotite inclusions and alteration to clay, and may be fractured and recrystallized micromosaics or preserve the relict forms of the volcanic protolith.

The biotite is of metamorphic origin, synkinematic, corresponds to microsheets of sizes smaller than 0.07 mm, brown in color, oriented in a lepidoblastic manner, and can appear in the limits of quartz mosaics, limiting the crystals, or in bands that indicate the schistosity of the rock. White mica is present in microcrystalline aggregates forming bands with biotite, developed by metamorphic recrystallization, or with the micromosaics of quartz and feldspars in the matrix.

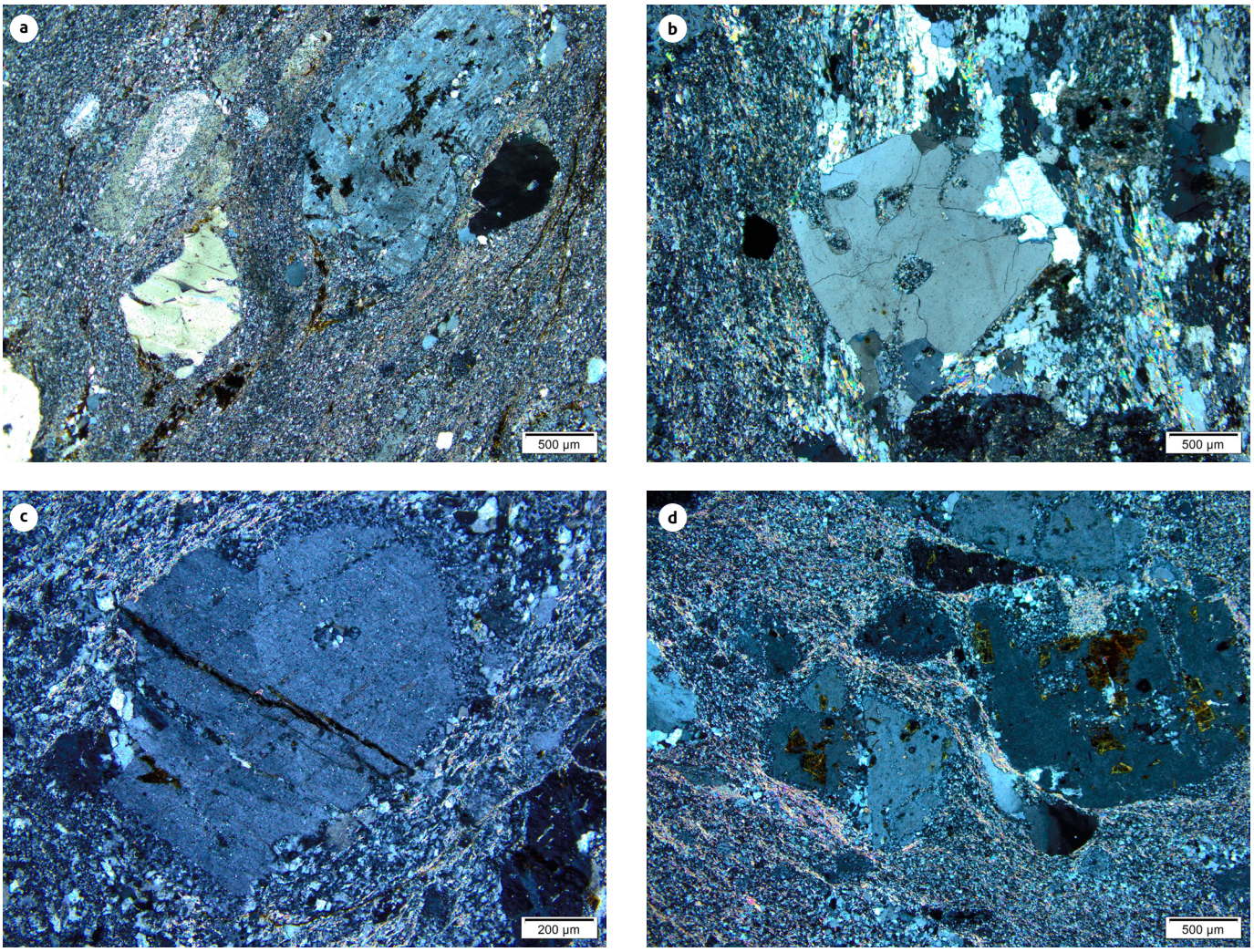

Figure 3. Microscopic aspect of quartz (Qz), plagioclase (Pl) and alkaline feldspar (Fsp) porphyroclasts within a microcrystalline matrix (M) Petrographic samples of the Onzaga Metarhyolite: a) Sample IGM-900893, porphyroclasts with development of augen forms and asymmetric tails. b) Sample IGM-900968, quartz porphyroclasts with bays and edges corroded by the matrix inherited from the protolith. c) Sample IGM-900913, alkaline feldspar porphyroclast with slight recrystallization at the edges and inside the crystal. d) Sample IGM-900928, deformed and recrystallized porphyroclasts along the edges.

The rock matrix presents different degrees of metamorphic recrystallization, depending on the rock. The matrix consists of felsitic microcrystalline mosaics of quartz, plagioclase and alkaline feldspar, with oriented microsheets of white mica and biotite in some rocks, which can form oriented bands that mark the schistosity of the rock. In some rock samples, the fluid structure of the vitreous protolith of rhyolitic composition is preserved but recrystallized to granoblastic micromosaics (Figure 4).

The rock preserves the porphyritic texture of the igneous protolith and some characteristics of the phenocrysts, but these rocks have been deformed and locally recrystallized by dynamic metamorphism, especially at the edges, in addition to being oriented in the direction of the metamorphic foliation. The recrystallization of feldspars and quartz and the formation of biotite and white mica by blasthesis suggest that this rock probably reached the low amphibolite facies. The rock has a schist metamorphic structure marked by biotite and white mica. The original matrix of the protolith recrystallized to a microgranoblastic felsitic mosaic, and oriented micaceous minerals with lepidoblastic texture were formed.

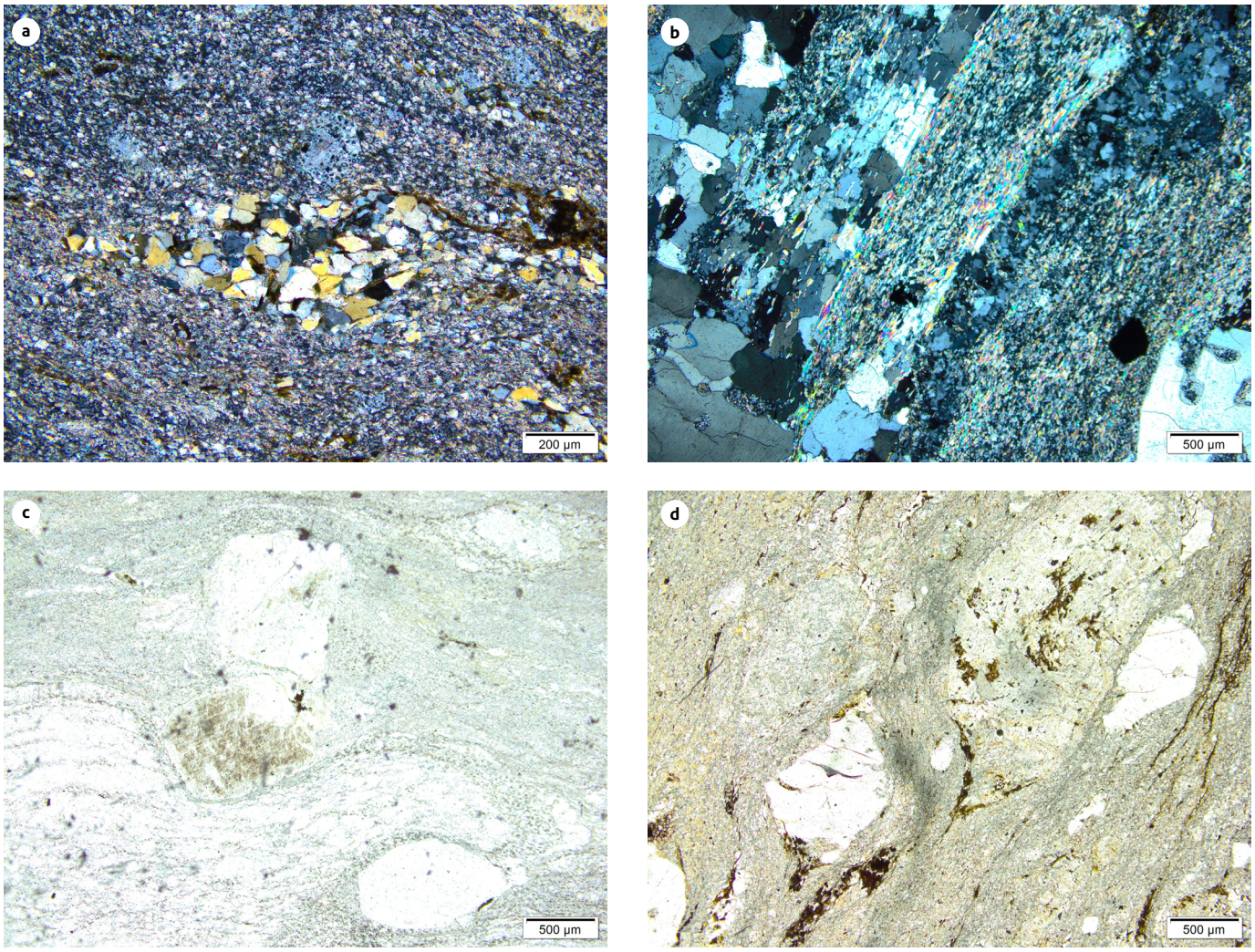

Figure 4. Characteristics of the rock matrix of the Onzaga Metarhyolite
a) Sample IGM-900893, quartz augen with polygonal microcrystals and oriented muscovite microsheets. b) Sample IGM-900968, fine bands in the recrystallized matrix with oriented muscovite interspersed with granoblastic bands of quartz and feldspars. c) Sample IGM-900992 and d) Sample IGM-900893, development of porphyroclasts in the form of asymmetric augens and slightly banded microcrystalline matrix.

4.2. Geochemistry

The geochemical analysis was performed on four rock samples distributed spatially in the body and classified petrographically as metarhyolite, metadacite and metaquartzlatite. The results are presented in Table 2, and the spatial distribution is shown in Figure 1.

The four samples have high SiO_2 contents, with values between 76.9% and 79.3%, low Fe_2O_3, TiO_2, CaO, MnO and MgO contents, and high K_2O values between 4.03% and 5.66% (Table 2). High values of Al_2O_3 (11.5% to 14.3%) and low values of $Fe_2O_3 + TiO_2 + MgO$ (1.18% to 2.04%) correspond to metarhyolites with few ferromagnesians. Losses on ignition (LOIs) are less than 1.62%, which suggests that they are slightly altered rocks, as shown in the petrographic analysis. The Onzaga Metarhyolite was subjected to metamorphism after crystallization, with the possibility of mobilizing major elements (Si, K, Na, Ca, Mg, and Fe) and large ion lithophiles (LILEs), such as Rb, Ba and Sr. In contrast, trace elements of small ionic radius, rare earths (REEs) and some transition metals (Ti, V, and Cr) have been considered immobile in postmagmatic conditions, such as metamorphism (Hastie et al., 2007; Winchester and Floyd, 1977).

Table 2. Content of major oxides in rocks of the Onzaga Metarhyolite

IGM	FIELD No.	SiO_2	TiO_2	Al_2O_3	Fe_2O_3	MgO	CaO	Na_2O	K_2O	P_2O_5	MnO	LOI
900893	GR-6733	76.86	0.13	13.17	1.70	0.05	0.23	2.35	5.40	0.10	0.005	0.95
900928	LMC-076	78.15	0.04	14.26	1.00	0.22	0.05	1.31	4.97	0.00	0	1.62
900968	TCR382	78.70	0.15	13.24	1.91	0.00	0.55	1.30	4.03	0.11	0.01	1.12
900992	JGB-483	79.32	0.07	11.53	1.12	0.00	0.00	2.30	5.66	0.00	0.002	0.54

The rocks of the Onzaga Metarhyolite plot in the rhyolite field in the diagram of Winchester and Floyd (1977) (Figure 5a). In the diagram of Th vs. Co, Hastie et al. (2007) plot in the field of andesites, departing from the petrographic classification, and correspond to calc-alkaline rocks with high K (Figure 5b). They have alkali values ($Na_2O + K_2O$) between 5.3% and 7.9% and $K_2O/Na_2O > 2$. They are classified within peraluminous rocks, with values of A/CNK> 1 and A/NK values between 1 and 2 (Shand diagram, 1943) (Figure 5c). The high contents of K_2O and moderate values of Na_2O correspond to magmas related to those that generate S-type granites, as shown in the diagram of Chappell and White (1974) (Figure 5d). The mineralogy of the rocks shows the development of white mica and subordinate biotite.

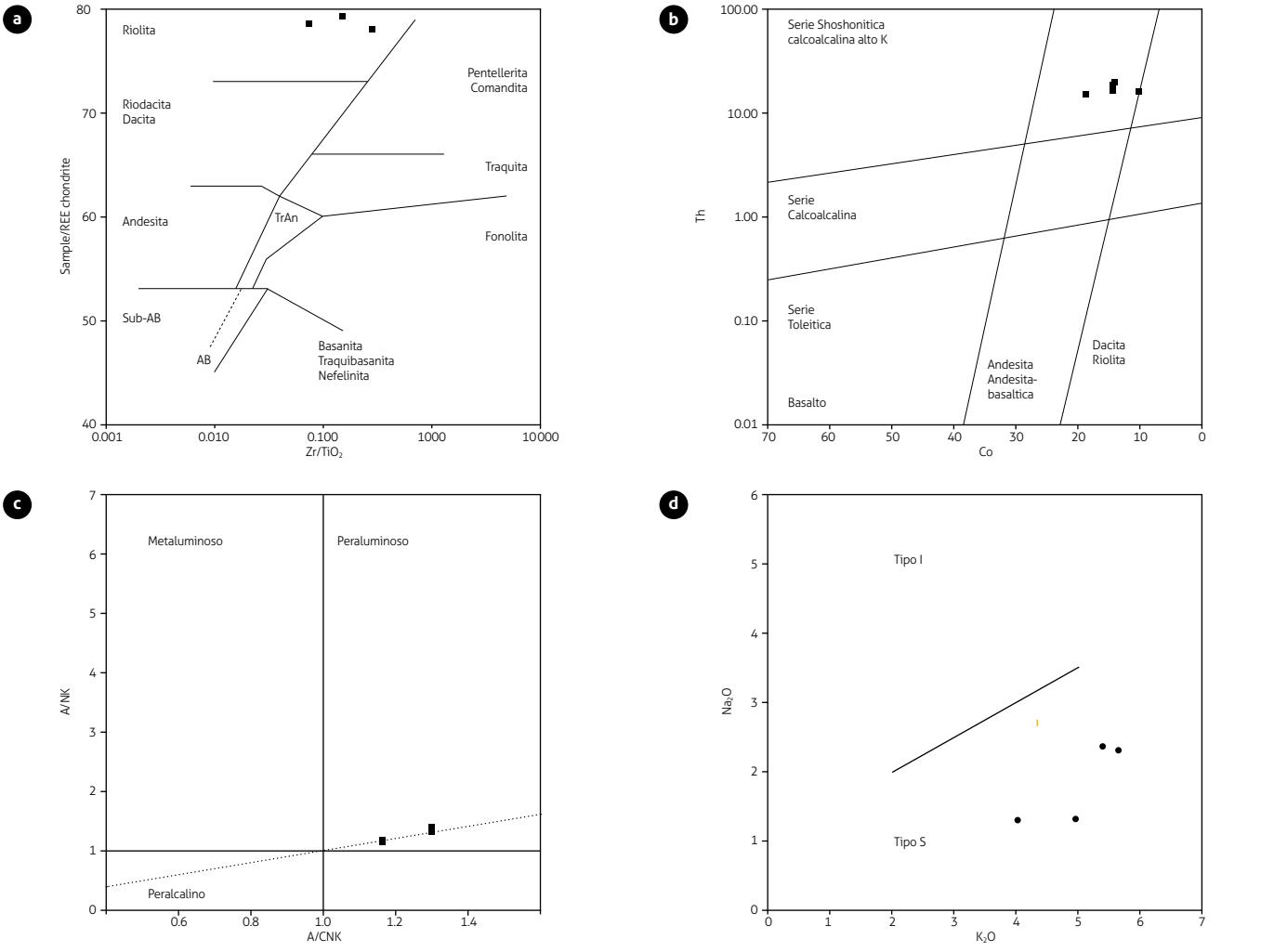

Figure 5. Classification diagram of volcanic rocks of the Onzaga Metarhyolite
a) Diagram of Zr/TiO_2 vs. SiO_2 (Winchester and Floyd, 1977). b) Co vs. Th diagram (Hastie et al., 2007). c) Shand classification diagram (1943). d) Diagram K_2O vs. Na_2O by Chappell and White (1974) to discriminate between type I and type S granites.

Table 3 summarizes the values of the trace elements. The contents of Rb, Sr, Ba and Zr vary from 218-256 ppm, 26-56 ppm, 167-1113 ppm and 105-114 ppm, respectively. The rocks are characterized by high Rb/Zr ratios (between 1.9 and 2.2), Rb/Ba ratios <0.29, except for sample JGB-483, which has a value of 2, and high Rb/Sr values (between 3.8 and 9.8).

The multielement diagram of trace elements normalized to the upper continental crust (Figure 6a) (Taylor and McLennan, 1995) in rocks of the Onzaga Metarhyolite shows negative anomalies of Sr and Ti that are related to minerals, such as plagioclase and Fe-Ti opaques, respectively (McDonough and Sun, 1995). Sample JGB-484 shows a negative Ba (113 ppm) anomaly. The negative anomalies of Ba, Sr and Eu may be related to the low modal proportion of plagioclase observed (Table 1), and it is likely that in the source, the plagioclase was in a slightly abundant phase. The other elements present values close to those of the upper continental crust.

The diagram of rare earth elements (REEs) normalized to chondrite according to the values of Nakamura (1974) (Figure 6b) presents enrichment in light rare earth elements (LREEs) of approximately 80 to 100 times with respect to the value of chondrite, with a pattern that is progressively impoverished toward heavy rare earth elements (HREEs). Additionally, they have negative Eu anomalies, with low Eu/Eu * values between 0.12 and 0.74. The negative Eu anomaly can be caused by early fractionation of plagioclase in the magma or fusion of previous

Table 3. Results of trace elements and rare earth elements in rocks of the Onzaga Metarhyolite

IGM	900893	900928	900968	900992
N field	GR-6733	LMC-076	TCR382	JGB-483
Li	15	7.3	17	3.8
Be	5.9	3.2	6.6	4.6
Sc	11	14	15	7.9
V	4.2	5.0	9.0	4.8
Cr	2.1	2.1	2.0	3.5
Mn	273	204	377	126
Co	10	14	19	14
Nor	1.7	2.5	3.621	<0.5
Cu	6.6	4.2	5.3	6.3
Zn	62	23	52	46
Ga	21	22	25	14
As	6.4	2.7	3.1	1.9
Rb	245	256	218	231
Sr	53	26	56	25
Y				26
Cd	0.14	<0.08	0.15	0.10
In	0.12	0.13	0.15	0.040
Cs	5.1	3.2	2.4	2.6
Ba	1167	856	991	113
La	44	33	39	25
Ce	79	74	75	58
Pr	12	9.9	9.9	7.7
Nd	45	31	36	27
Sm	12	8.2	9.6	6.3
Eu	1.6	0.98	1.9	0.23
Gd	9.2	4.3	6.5	5.2
Tb	2.3	0.57	1.5	0.88
Dy	15	1.9	6.6	4.8
Ho	2.9	0.33	1.2	0.94
Er	8.5	1.1	3.2	2.8
Tm	1.18	0.12	0.41	0.40
Yb	7.3	0.91	2.7	2.7
Lu	0.96	0.14	0.42	0.39
Tl	1.5	1.4	1.0	1.2
Pb	24	15	25	27
Bi	0.23	0.43	0.70	0.055
Th	16	17	15	20
U	3.1	2.7	4.0	4.1
Zr	109	114	111	105
Nb	27	27	23	25
W	37	43	68	63

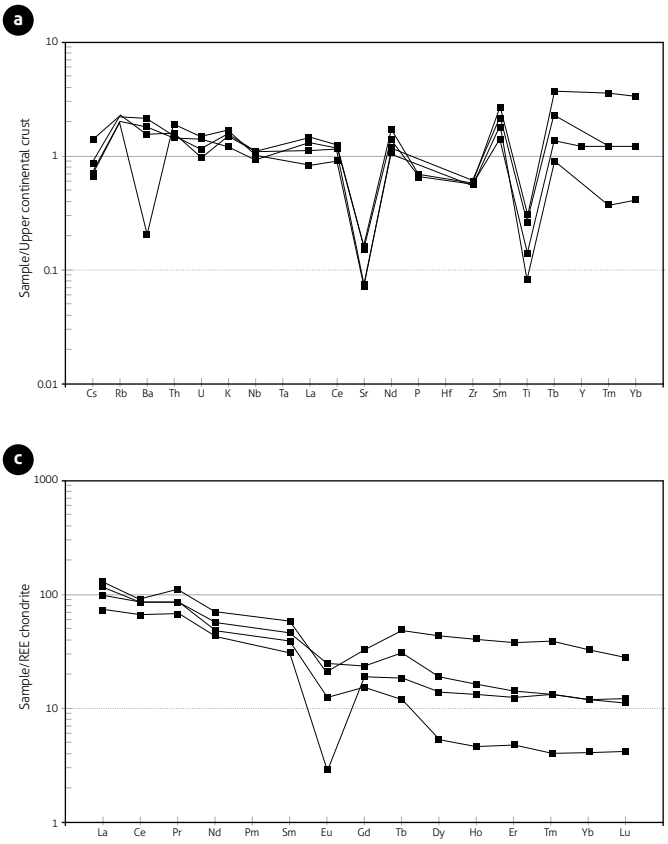

Figure 6. Multielement diagrams for rocks of the Onzaga Metarhyolite
a) Diagram of trace elements normalized to the upper crust (Taylor and McLennan, 1995); b) Rare earth element diagram (REE) normalized to the Nakamura chondrite (1974).

igneous rocks with negative Eu anomalies; however, it is not easy to determine the reasons for the behavior of the plagioclase in the source area or the subsequent removal of plagioclase phenocrysts from the melt. When comparing the average value of Eu/Eu * (0.56) in rocks of the Onzaga Metarhyolite with the average values obtained by Tang et al. (2015) for the upper crust (0.67 ± 0.01), the values are slightly lower but close to the average value of the upper crust. The normalized values of $(La/Yb)_N$ vary between 4 and 24.4; $(La/Sm)_N$ varies between 2.2 and 2.5; and $(Eu/Yb)_N$ varies between 0.2 and 2.1.

4.3. Geochronology

For the geochronological analysis of the Onzaga Metarhyolite, two rocks were analyzed by the U-Pb LA-ICPMS method in zircons. The ages are summarized in Table 4, the spatial location is shown in Figure 1, and the results are presented in Supplementary Data. The reported ages are calculated with the Pb^{206}/U^{238} ratio. In the calculation of the crystallization age of each rock, the presence or absence of populations is considered according to the probability density diagram and the distribution in the concord diagram.

Sample JGB-483 was chemically classified as a rhyolite with quartz, plagioclase and sanidine porphyroclasts that correspond to 14.9% of the rock. The matrix is microgranoblastic and occupies the remaining 85.1%. The rock partially preserves the flow structure of the volcanic protolith, being constituted by cryptocrystals and microcrystals of quartz, feldspars and sericite, with schist structure and thicker recrystallized sectors with polygonal textures combined with thinner bands. Most of the zircons in the sample are short and prismatic, with pyramidal ends smaller than 50 µm. The cathodoluminescence images are of very low quality and do not allow us to define the internal structure of each zircon or the presence of inherited nuclei, but in some cases, the concentric structure of igneous zircons is recognized. The ablations were advanced in the zircon nuclei. To determine ages, a total of 47 analyses were performed; 5 analyses had discordances > 5, and 12 analyses did not touch the concord curve and were eliminated (Figure 7).

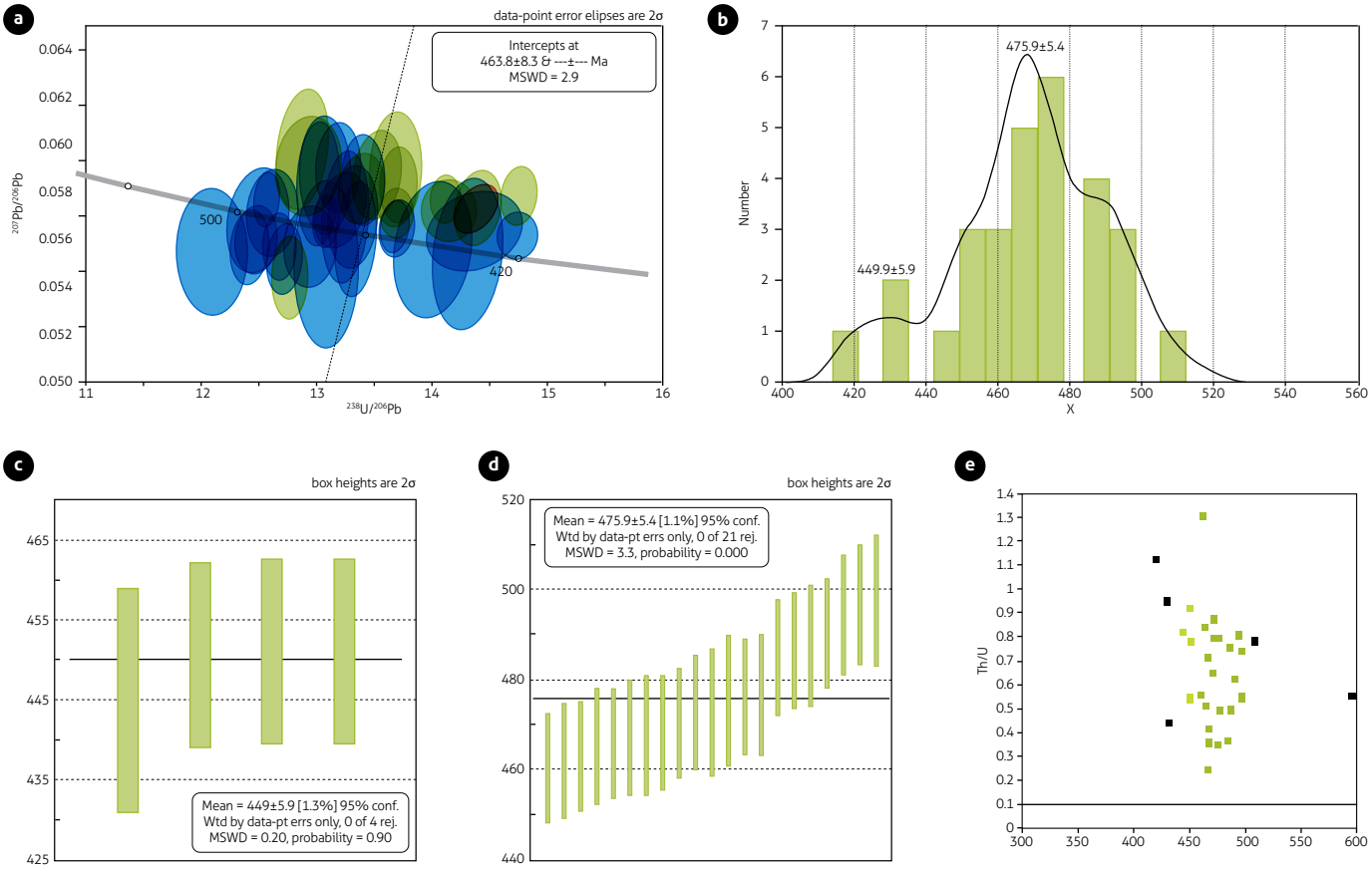

Figure 7. Results of U-Pb dating in zircon of sample JGB-483
a) Concordia Tera-Wasserburg; blue is accepted data, green is deleted data; b) Probability density diagram; c) Weighted average age. e) Age-Th/U relationship.

The accepted analyses show a wide dispersion between 419.5˚±˚11.06 Ma and 509.1 ± 15.8 Ma. A weighted average age was obtained from four concordant analyses that yielded 449.9 ± 5.9 Ma with an MSWD = 0.20, which is interpreted as the age of rock crystallization, and an inherited age was obtained from 21 accepted analyses, with Pb^{206}/U^{238} values that yielded an age of 475.9 ± 5.4 Ma and MSWD = 3.3. Additionally, in the range of all the results between 445 ± 14 and 497.7 ± 14.6 Ma, an integrated age of 471.2 ± 6 Ma was obtained with MSWD = 5.3. The Th/U ratio> 0.1 for all accepted zircons suggests that they correspond to zircons formed from a melt (Rubatto, 2002).

A second sample (LMC-076) was analyzed, which corresponds to a metarhyolite with quartz porphyroclasts, plagioclase and alkali feldspar and recrystallization at the edges. The porphyroclasts are distributed within the oriented microcrystalline matrix, which is mainly composed of quartz and sericite. The zircons are prismatic, elongated and short, and some are small, rounded, and lilac. They are located in the rock matrix and are smaller than 50 μm. The cathodoluminescence images show a concentric structure of igneous zircons, with some inherited dark-gray nuclei and more luminescent light-gray edges.

To determine ages, 60 analyses were performed (Supplementary Data), of which 8 were eliminated with discordances > 5 and errors > 4.5 (Figure 8). A zircon crystal is presented with two analyses that yield results of 188.4 ± 4 Ma and 190.3 ± 5 Ma, which is interpreted as a contaminating zircon that is probably associated with the Triassic-Jurassic magmatism of the Santander massif. A population is presented with ages between 430.5 ± 9 Ma and 458.3 ± 7 Ma that determine the average age of rock crystallization as 450.9 ± 2.5 Ma, MSWD = 2.5 (n = 29). A second population of xenocrysts, with ages between 462.4 ± 8 Ma and 479 ± 10 Ma, showed an average age of 469.8 ± 4.0 Ma, MSWD = 4 (n = 9) and presents xenocrysts and inherited nuclei of the Neoproterozoic, with two data points of 555 ± 11 Ma and 565.7 ± 9 Ma, a population of three data points with an average age of 617 ± 16 Ma and MSWD = 1.7. A population of three data points, with an average age of 644, 5 ± 6.5 Ma and MSWD = 0.067 and three heritages, occurred between 1071 ± 48 Ma and 1171 ± 37 Ma. The Th/U ratio of these heritages is greater than 0.1, which suggests that the inherited zircons are igneous (Rubatto, 2002).

5. Discussion

5.1. Correlations and Ordovician magmatism

Two populations of Ordovician igneous ages were found in the two analyzed samples from the Onzaga Metarhyolite: in sample JGB-483, the youngest average age yielded a value of 449.9 ± 5.9 Ma (n = 4), and the second population showed an average age of 475.9 ± 5.4 Ma (n = 21); in the LMC-076 sample, the average age of rock crystallization is 450.9 ± 2.5 Ma (n = 29), and the second igneous population is 469.8 ± 4.0 (n = 9). The results in both samples are comparable and suggest that the crystallization age of the rhyolitic lavas occurred at approximately 450 Ma (Upper Ordovician), while the second age corresponds to a population of inherited magmatic zircons with ages of approximately 470-475 Ma (Lower-Middle Ordovician limit), which is interpreted as zircons contributing to the rhyolitic magma, possibly as a result of the fusion of crustal rocks that crystallized during the Lower-Middle Ordovician.

Figure 9 shows a correlation graph of U-Pb ages for different Ordovician units of the Santander and Floresta massifs and the Mérida Mountain range, and Table 4 summarizes the ages with which the figure was made.

In the Santander massif, the Onzaga Metarhyolite presents ages slightly older than the crystallization of the Durania, Timotes and Tarra granites and agrees with the K-Ar age in muscovite of a pegmatite that cuts the Bucaramanga gneiss to the east of the town of Chitagá, with 457 ± 13 Ma (Goldsmith et al., 1971), as well as with a gabbro unit that outcrops near Pamplona, which yields a K-Ar age in total rock of 456 ± 23 Ma (Boinet et al., 1985); this age is slightly younger than the U-Pb age reported for the Santa Rosita Monzogranite of 460.2 ± 4.6 Ma (Zapata et al., 2017) and that of a granofels that corresponds to a xenolith of an orthogneiss within the Monzogranite of La Corcova, which gave a U/Pb crystallization age of 462.7 ± 3.1 Ma (Rodríguez et al., 2017a, 2020). The Berlin orthogneiss has a similar U/Pb crystallization age of 451.5 ± 1.3 Ma (van der Lelij et al., 2016) (Table 4, Figure 9).

In the Mérida Mountain range, the Onzaga Metarhyolite is geochronologically correlated with the Verdalito, Macanas, Chapolo, Miraflores, Carmania and La Puerta granitoids, with the orthogneiss units of La Raya, Micarache and La Playita, with the Iglesias Complex and with the Bailadores rhyolite. All these units, with similar U/Pb ages, were reported by van der Lelij et al. (2016) and Tazzo et al. (2018) (Table 4, Figure 9). The Onzaga Metarhyolite has slightly younger ages than the

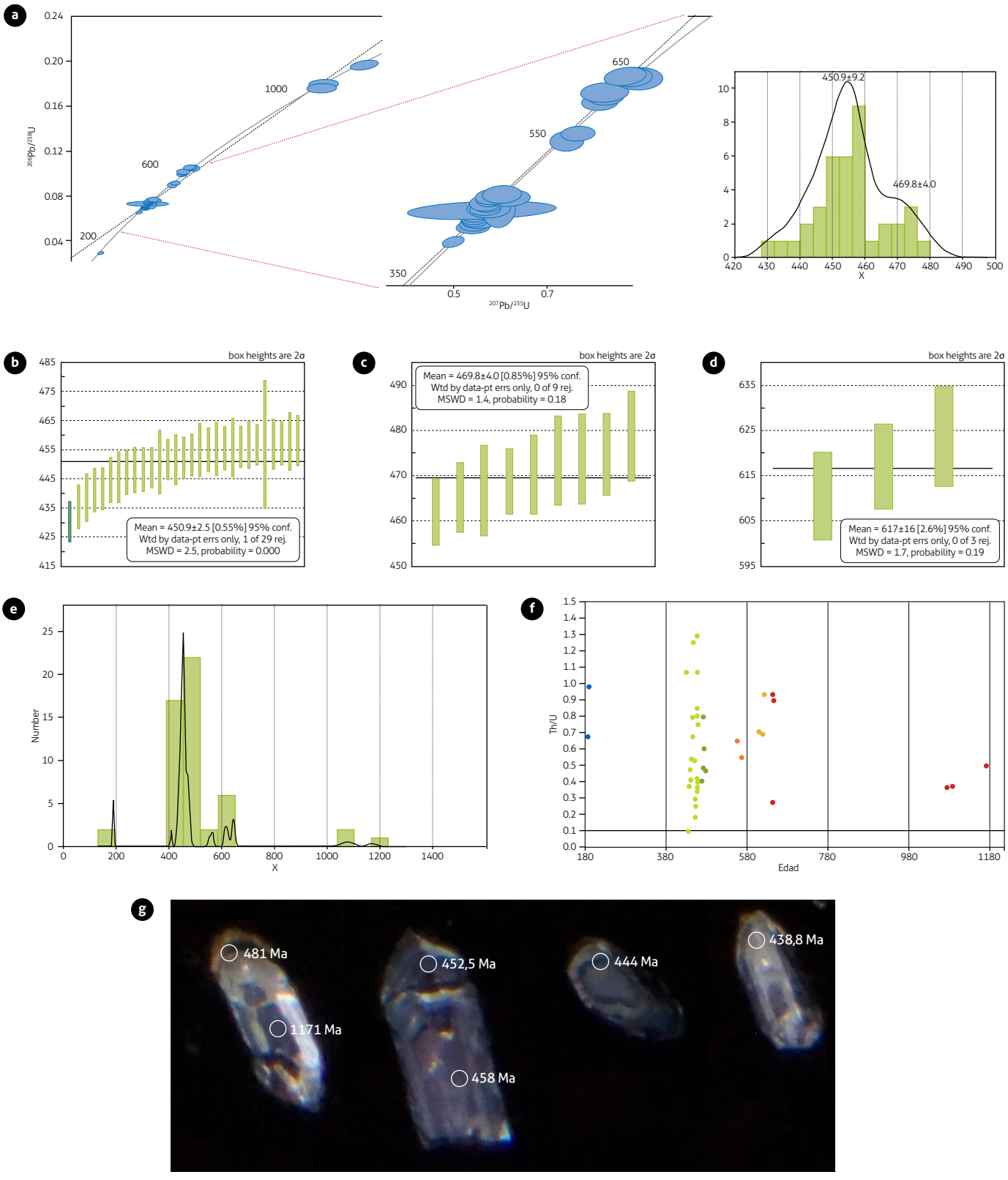

Figure 8. Results of U-Pb dating in the zircon of sample LMC-076
a) Concordia Tera-Wasserburg; b) Probability density diagram; c) Weighted average age diagrams; e) Diagram of probability density in inherited zircons; f) Age-Th/U relationship; g) Cathodoluminescence images of zircons from sample LMC-076.

Mitisus gneiss. In the Floresta massif, the ages reported for the Santa Rosita Monzogranite are slightly older than those of the Onzaga Metarhyolite but could be related to the same magmatism (Table 4, Figure 9).

The Ordovician ages inherited from the Onzaga Metarhyolite (*ca.* 470-475 Ma, lower-middle Ordovician limit) are comparable with ages obtained in the Santander massif in nonfoliate granitoid rocks of 471 ± 7 Ma (Restrepo-Pace and Cediel, 2010). Within the foliated bodies, there are U/Pb ages of 473.5 ± 2.5 Ma and 472.5 ± 3.4 Ma in the orthogneiss of Berlin, 479 ± 10 and 471 ± 11 in the gneiss of Bucaramanga (van der Lelij et al., 2016; García Ramírez et al., 2017), and an age of 477.0 ± 5.3 in a paragneiss migmatite (van der Lelij, 2013; van der Lelij et al., 2016). Although they are foliated rocks, the U-Pb ages in zircon presented by the aforementioned authors were interpreted as those of crystallization and have Th/U ratios > 0.1.

Table 4. U-Pb ages in zircon for different Ordovician bodies of the Santander, Floresta, Quetame and Mérida Mountain ranges

No. field	Coordinates		Unity	Age U/Pb (Ma)	MSWD	Source
	West (m)	North				
Mérida Mountain range						
08VDL03	8° 28' 49"	71° 34' 13"	Verdalite granodiorite	449.3 ± 2.5	2	Van der Lelij et al. (2016)
08VDL11	8° 41' 41"	70° 53' 31"	Micarache orthogneiss	454.0 ± 10.0	2.5	Van der Lelij et al. (2016)
08VDL15	8° 11' 51"	71° 50' 09"	Alkali rhyolite dancers	452.6 ± 2.7	2.7	Van der Lelij et al. (2016)
08VDL21	8° 08' 28"	71° 56' 15"	La Grita Diorite	471.8 ± 4.0	2	Van der Lelij et al. (2016)
08VDL22	8° 11' 38"	71° 53' 02"	La Playita orthogneiss	449.7 ± 4.4	9.3	Van der Lelij et al. (2016)
08VDL36	8° 27' 53"	71° 26' 50"	Puente Real augen gneiss	472.3 ± 3.4	4.1	Van der Lelij et al. (2016)
08VDL38	8° 20' 19"	71° 37' 21"	Macanas alkali granite	454.8 ± 4.2	1.5	Van der Lelij et al. (2016)
08VDL41	8° 55' 55"	70° 47' 31"	Chapolo Granite	454.5 ± 3.1	1	Van der Lelij et al. (2016)
08VDL44	9° 10' 42"	70° 38' 08"	Miraflores granodiorite	447.9 ± 2.5	1.4	Van der Lelij et al. (2016)
08VDL47	9° 15' 59"	70° 38' 18"	Carmania monzodiorite	450.4 ± 2.5	1.5	Van der Lelij et al. (2016)
08VDL49	9° 07' 11"	70° 42' 39"	La Puerta Granodiorite	453.1 ± 1.8	2.1	Van der Lelij et al. (2016)
QG-25	8° 41' 37"	70° 56' 23"	Complex churches	451.4 ± 3.6	0.69	Tazzo et al. (2018)
QM-02	8° 44' 23"	70° 53' 49"	Complex churches	435.5 ± 5.9	0.81	Tazzo et al. (2018)
GLR-02c	8° 54' 0"	70° 37' 43"	The hornblende-gneiss ray	458.0 ± 3.4	0.53	Tazzo et al. (2018)
SB-0405	8° 52' 7"	70° 35' 30"	Mitisus gneiss	466.8 ± 3.7	0.69	Tazzo et al. (2018)
SDB-01	8° 52' 38"	70° 38' 4"	Complex churches	487.2 ± 7.0	0.97	Tazzo et al. (2018)
CM-01	8° 42' 20"	70° 50' 15"	Sierra Nevada	445 ± 31	0.64	Tazzo et al. (2018)
Santander Massif						
10VDL49	7° 29' 20"	72° 42' 16"	Fm Silgará	479.8 ± 3.1	1.7	Van der Lelij et al. (2016)
10VDL47	7° 28' 23"	72° 41' 44"	Gabbrodiorite	483.7 ± 5.9	0.7	Van der Lelij et al. (2016)
10VDL46	7° 16' 29"	72° 39' 55"	Durania granite	439.2 ± 4.7	8	Van der Lelij et al. (2016)
08VDL50	9° 00' 52"	70° 44' 25"	Timotes granite	445.2 ± 3.9	8.2	Van der Lelij et al. (2016)
GE-58-M1	7° 23' 27.6"	72° 53' 28.7"	Foliate metadiorites	477.0 ± 4.1	2.9	Mantilla et al. (2012)
GH-72-M2	7° 23' 27.6"	72° 53' 28.7"	Foliate metadiorites	477 ± 2	4.7	Mantilla et al. (2012)
GI-60-M2	7° 23' 27.6"	72° 53' 28.7"	Foliate metadiorites	481.9 ± 6.1	4.1	Mantilla et al. (2012)
10VDL50	7° 15' 22"	72° 53' 45"	Migmatite from paragneiss	477.0 ± 5.3	7.5	Van der Lelij et al. (2016)
10VDL23	6° 56' 35"	72° 58' 00"	Bucaramanga gneiss	461 ± 2.1	2.6	Van der Lelij et al. (2016)
VR-7-2	7° 10' 29.40"	72° 42' 07.15"	Bucaramanga gneiss	479 ± 10		García Ramírez et al. (2017)
VR-22-1	7° 12' 11.95"	72° 46' 49.22"	Bucaramanga gneiss	471 ± 11		García Ramírez et al. (2017)
10VDL51	7° 15' 17"	72° 53' 48"	Orthogneiss of Berlin	472.5 ± 3.4	11.5	Van der Lelij et al. (2016)
10VDL37	7° 11' 24"	72° 58' 41"	Orthogneiss of Berlin	451.5 ± 1.3	1	Van der Lelij et al. (2016)
10VDL44	7° 20' 40"	72° 42' 59"	Orthogneiss of Berlin	473.5 ± 2.5	4.6	Van der Lelij et al. (2016)
10VDL55	8° 03' 10"	73° 04' 31"	Tarra granodiorite	443.4 ± 3.2	3.8	Van der Lelij et al. (2016)
AMC-0128A	7° 08' 12.59"	73° 02' 17.97"	Xenolith-granofels of Qtz-Pl-Kfs	462.7 ± 3.1	1.7	Rodríguez et al. (2020)
JGB-483	6° 11' 05.98"	72° 50' 23.61"	Onzaga Metarhyolite	449.9 ± 5.9	0.2	This work
LMC-076	6° 21' 00.88"	72° 49' 18.27"	Onzaga Metarhyolite	450.9 ± 2.5	2.5	This work
Massif of Floresta and Quetame						
RH1	4° 23' 1085"	73° 17' 24.95"	Granodiorite mine	483 ± 10	4.2	Horton et al. (2010)
FS11A	5° 50' 55.53"	72° 51' 52.12"	Otengá stock	482 ± 15	6.5	Horton et al. (2010)
1308080	5° 58' 54.44"	72° 48' 45.84"	Otengá stock	477 ± 11	28	Horton et al. (2010)
GZ-6837	6° 13' 13.93"	72° 47' 04.91"	Monzogranite from Santa Rosita	479.0 ± 3.6	1.2	Zapata et al. (2017)
JGB-482	6° 00' 50.37"	72° 52' 35.16"	Monzogranite from Santa Rosita	460.6 ± 4.6		Zapata et al. (2017)

Source: Rodríguez et al. (2020), Horton et al. (2010), Mantilla et al. (2012), van der Lelij et al. (2016), Zapata et al. (2017), García Ramírez et al. (2017), and Tazzo et al. (2018).

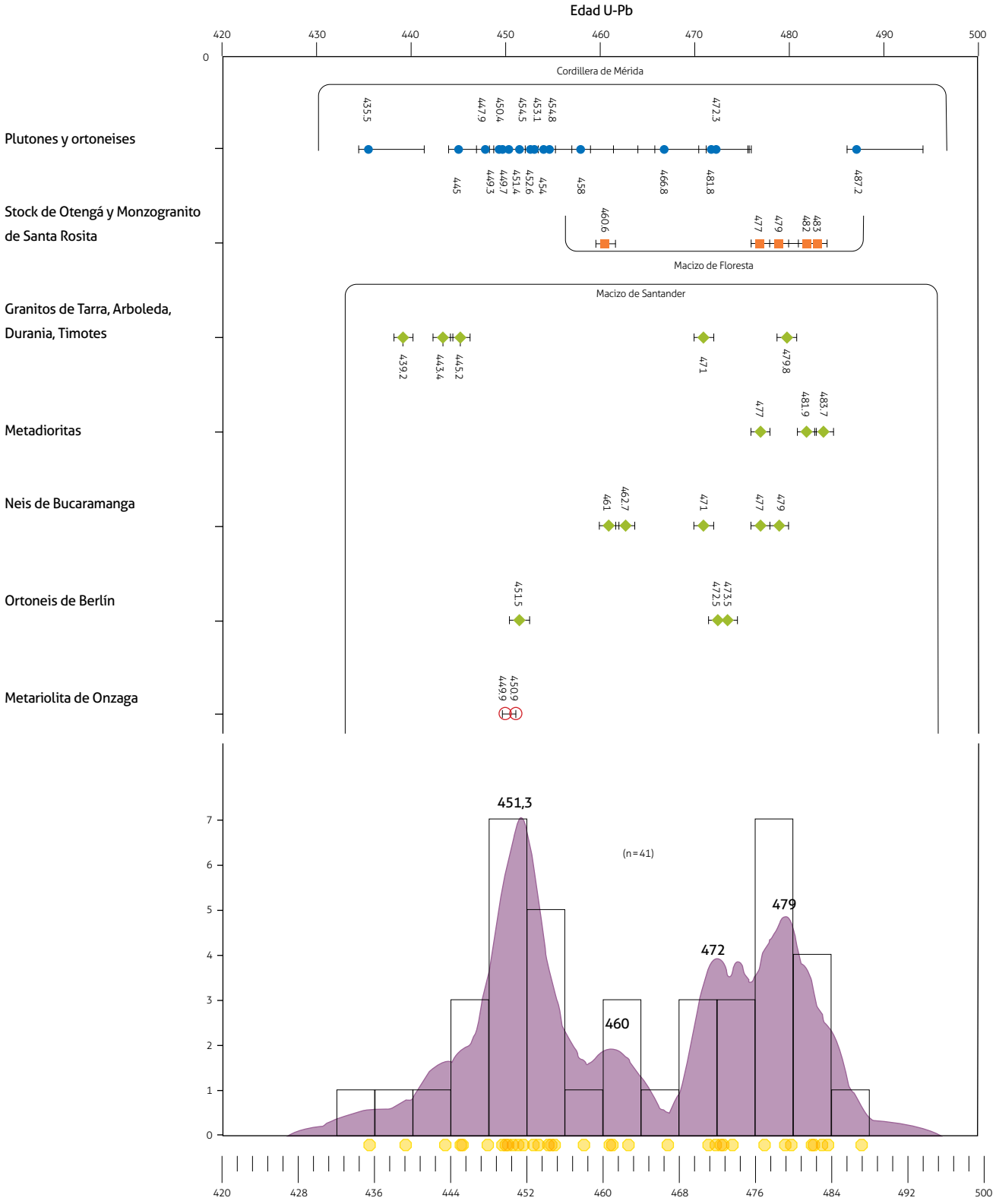

Figure 9. Compilation of U-Pb ages of different Ordovician bodies of the Santander, Floresta, Quetame and Mérida Mountain ranges and kernel density estimation diagram for crystallization ages of Ordovician units
Source: Rodríguez et al. (2020), Horton et al. (2010), Mantilla et al. (2012), van der Lelij et al. (2016), Zapata et al. (2017), García Ramírez et al. (2017), and Tazzo et al. (2018).

Some units have slightly older ages, such as the Otengá Stock in the Floresta massif with U-Pb ages of 477 ± 11 Ma and 482 ± 15 Ma (Horton et al., 2010); the bodies of metadiorites and gabbrodiorites give U/Pb ages of 477.0 ± 4.1 Ma, 477 ± 2 Ma, 481.9 ± 6.1 Ma and 483.7 ± 5.9 Ma (Mantilla et al., 2012; van der Lelij et al., 2016), which represents a more basic magmatism than that of orthogneiss and nonfoliated granites, which are younger.

Further west, in the Central Cordillera of Colombia, Martens et al. (2014) recorded igneous U-Pb ages of the La Miel gneiss of 479 + 15/-1 Ma (n = 7) and 443 ± 8 Ma (n = 8), the latter in the zircon magmatic edges, associated with the Anacona terrain, which for these authors represents a portion of the Ordovician magmatic belt that bordered Gondwana in the early Paleozoic. As potential regional correlations, Martens et al. (2014), van der Lelij et al. (2016) and Tazzo et al. (2018) consider similarities with the first Paleozoic component of the Marañón Complex of Peru, the Acatlán Complex of the Mixtec terrain in southern Mexico and the Maya Block of Central America.

When analyzing Figure 9 and Table 4, it can be concluded that the magmatism of the Santander, La Floresta, Quetame and Mérida Mountain ranges presents at least four main crystallization events in the Ordovician, which can be grouped at approximately 479-472 Ma, *ca.* 460 Ma and *ca.* 451 Ma. In the interval between 479-472 Ma, basic to intermediate magmatism is recognized in the Santander massif at approximately 479 Ma (diorites and gabbrodiorites), which formed small calc-alkaline intrusions and have been interpreted by Mantilla et al. (2012) as plutons formed from magmas derived from the mantle; this finding is possibly associated with a suprasubduction event related to the beginning of the closure of the Lapetus Ocean. In this same interval but approximately 472 Ma, felsic bodies, calc-alkaline high in K, peraluminous and migmatitic gneiss (orthogneiss of Berlin and gneiss of Bucaramanga) were formed; these formations have been explained by partial fusion of continental crust, producing felsic magmatic rocks, likely facilitated by the heat transfer of basic magmas at the base of the crust (Huppert and Sparks, 1988; Cochrane et al., 2014; van der Lelij, 2016) and by the existence of an active continental margin. This process occurred between *ca.* 495 Ma and *ca.* 415 Ma (van der Lelij et al., 2016). These rocks are part of the Famatinian Arc that crops out south of the continent. Subsequently, a discrete crystallization event of approximately 460 Ma is recognized (Santa Rosita Monzogranite, Qtz-Fsp-Pl granofels xenolith within the La Corcova Monzogranite and an age in the Bucaramanga gneiss), which continues to be magmatic, high calc-alkaline K and peraluminous. At approximately 451 Ma, one of the largest magmatism and crystallization events occurred, with the formation of volcanic rocks (Onzaga Metarhyolite) that were probably fissurally extruded along faults based on the shape of the body, which is elongated and thin and has a N-S orientation. Contemporaneous with the volcanism, the intrusion of granite bodies (granites of Durania, Timotes and Tarra) occurred, being of acid magmatism, calc-alkaline high in K, peraluminous and of type S, with abundant contribution of zircons inherited from the igneous event of *ca.* 472-475 Ma, as evidenced by the geochronological results of the Onzaga Metarhyolite.

Trace elements in granitic magmas are dictated not only by the composition of the source but also by magmatic processes, such as partial melting and fractional crystallization. Therefore, they have little capacity to identify the nature of the source of the granites (Gao et al., 2016). The rocks of the Onzaga Metarhyolite and the Santa Rosita Monzogranite are distributed in the La/Sm vs. La diagram (Figure 10a) in the fields of partial fusion and fractional crystallization, while the samples of the Durania Granite plot in the rock field, as they were formed by partial fusion. The metasedimentary protolith granites can show compositional variations similar to the so-called peraluminous type I granites. The chemistry of these three units corresponds to peraluminous magmas, which plot in conventional diagrams in the field of S-type granites (Figure 10b), with two micas but whose source does not necessarily correspond to the melting of sediments or metasediments.

The presence of an abundant population of zircons with ages between 460 Ma and 497 Ma, Th/U ratios > 0.1 and a concentric structure suggests that the source of the Onzaga Metarhyolite corresponds to igneous rocks, with crystallization ages between 470 Ma and 475 Ma. The inheritances of xenocrysts and zircon nuclei with the Neoproterozoic results (Tonian, Cryogenian and Ediacarian) could be contributed by igneous sources rather than by the fusion of metasedimentary rocks. Considering that peraluminous magmas have a low capacity to melt zircons, this finding is attributable to the following factors: (1) the relatively high abundance of zircons in the case that they come from clastic metasedimentary rocks; (2) the relatively low temperatures for magmas with S-type granitics (Chappell et al., 2004); (3) the low solubility of zircon in peraluminous melts (Watson and Harrison, 1983); and (4) the

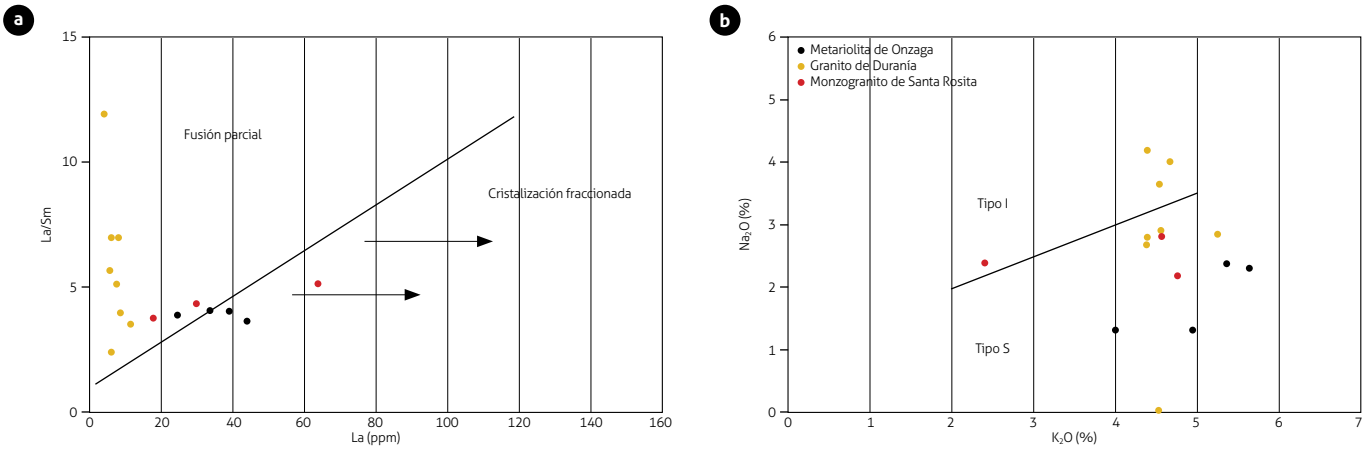

Figure 10. La-La/Sm diagram (Jiang et al., 2005): evolution of the magmas of the Onzaga Metarhyolite, Santa Rosita Monzogranite and Durania Granite by partial fusion. K_2O-Na_2O diagram of granite type classification (Chappell and White, 1992)

rapid migration of granitic magmas from the melting regions to the sites of emplacement (Clemens, 2003). Therefore, information on the nature of the source of the granites can be obtained by comparing magmatics zircons with inherited zircons (Jeon et al., 2012). In this sense, the inheritances of zircons in the Onzaga Metarhyolite point to an igneous source with magmatic zircons with average ages between~ 470 and~ 475 Ma, similar to the ages reported for the orthogneiss of Berlin and the gneiss of Bucaramanga.

6. Conclusions

New U-Pb LA-ICPMS geochronology data in zircons indicate volcanism *ca.* 451 Ma (Onzaga Metarhyolite) in the Santander massif, contemporaneous with plutonic bodies that crystallized in the Mérida Mountain range and the Santander massif itself. The volcanism results are acidic, high in K, peraluminous and of type S, with abundant contributions of zircons inherited from an igneous event *ca.* 472-475 Ma, which suggests the fusion of igneous rocks with these ages in the development of the magma that gave rise to the protolith of the metarhyolites.

In the Santander, La Floresta, Quetame and Mérida Mountain ranges, at least four crystallization events occurred during the Ordovician period, grouped *ca.* 479-472 Ma, *ca.* 460 Ma, and *ca.* 451 Ma, plus basic to intermediate magmatism at approximately 479 Ma. The crystallization of the Onzaga Metarhyolite is associated with rocks from *ca.* 451 Ma.

The volcanic rocks of the Onzaga Metarhyolite, after magmatic crystallization, were subjected to metamorphism that reached the green schist facies and probably reached the low amphibolite facies, as indicated by recrystallization of the edges of the quartz phenocrysts, plagioclase and alkali feldspar in some rocks. The metamorphism had a dynamic component, with the development of porphyroclasts with asymmetric tails and was generated by blasthesis microsheets of biotites and white mica that mark the foliation of the rocks.

Acknowledgments

Thank you to the following people and organizations: the Servicio Geológico Colombiano, who financed the study; the chemistry, thin section and geochronology laboratories of the Servicio Geológico Colombiano; geologists Gilberto Zapata, Tomás Correa, Lina Cetina and José Gilberto Bermúdez for their help with field sampling; and Tomás Correa for translation of the abstract and to the anonymous reviewers for their comments, which allowed us to improve the manuscript.

Supplementary Data

Supplementary data for this article can be found online at https://doi.org/10.32685/0120-1425/bol.geol.48.2.2021.571

References

Boinet, T., Bourgois, J., Bellon, H., & Toussaint, J. (1985). Age et repartition du Age et répartition du magmatisme Précénozoïque des Andes de Colombie=Age and distribution

of the Premesozoic magmatism of the Andes of Columbia. *Comptes-rendus des séances de L'Académie des Sciences. Serie 2, Mécanique- Physique, Chimie, Sciences des L'univers, Sciences de la Terre*, *300*(2), 445-450.

Castaño, J. M., Rodríguez F., & García, C. A. (2018). Caracterización de parámetros en la concentración de circones para andesitas, monzogranitos, riolitas, cuarcitas y cuarzomonzonitas. *Boletín Geológico*, (44), 25-38. https://doi.org/10.32685/0120-1425/boletingeo.44.2018.6

Cediel, F., Shaw, R. P., & Caceres, C. (2003). Tectonic assembly of the Northern Andean Block. In C. Bartolini, R. T. Buffler, & J. Blickwede (eds.), *The Circum-Gulf of Mexico and the Caribbean: Hydrocarbon Habitats, Basin Formation, and Plate Tectonics* (vol. 79, pp. 815-848). AAPG Memoir.

Chappell, B. W., & White, A. J. R. (1974). Two contrasting granite types. *Pacific Geology*, *8*(2), 173-174.

Chappell, B. W., & White, A. J. R. (1992). I- and S-type granites in the Lachlan Fold Belt. *Earth and Environmental Science Transactions of the Royal Society of Edinburgh*, *83*(1-2), 1-26. https://doi.org/10.1017/S0263593300007720

Chappell, B. W., White, A. J. R., Williams, I. S., & Wyborn, D. (2004). Low- and high-temperature granites. *Transactions of the Royal Society of Edinburgh: Earth Sciences*, *95*, 125-140. https://doi.org/10.1017/S0263593300000973

Clavijo, J., Mantilla, F. L. C., Pinto, J., Bernal, L., & Pérez, A. (2008). Evolución geológica de la serranía de San Lucas, norte del valle medio del Magdalena y noroeste de la cordillera Oriental. *Boletín de Geología*, *30*(1), 45-62.

Clemens, J. D. (2003). S-type granitic magmas-petrogenetic issues, models and evidence. *Earth-Science Reviews*, *61*(1-2), 1-18. https://doi.org/10.1016/S0012-8252(02)00107-1

Cochrane, R., Spikings, R., Gerdes, A., Winkler, W., Ulianov, A., Mora, A., & Chiaradia, M. (2014). Distinguishing between in-situ and accretionary growth of continents along active margins. *Lithos*, *202-203*, 382-394. https://doi.org/10.1016/j.lithos.2014.05.031

Correa-Martínez, A. M., Rodríguez, G., Arango, M. I., Zapata, G., & Bermúdez J. G. (2017). *Catálogo de unidades litoestratigráficas de Colombia. Batolito de Mogotes*. Servicio Geológico Colombiano.

Coyner, S. J., Kamenov, G. D., Mueller, P. A., Rao, V., & Foster, D. A. (2004). FC-1: A zircon reference standard for the determination of Hf isotopic compositions via laser ablation ICP-MS. *American Geophysical Union, Fall Meeting Abstracts.*

Frost, B., & Frost. D. (2008). A geochemical classification for feldspathic igneous rocks. *Journal of Petrology*, *49*(11), 1955-1969. https://doi.org/10.1093/petrology/egn054

Gao, P., Fei Zheng, Y., & Fu Zhao, Z. (2016). Distinction between S-type and peraluminous I-type granites: Zircon versus whole-rock geochemistry. *Lithos*, *258-259*, 77-91. https://doi.org/10.1016/j.lithos.2016.04.019

García Ramírez, C., Rey-León, V., & Valencia, V. (2017). Ortoneises en la Franja Silos-Babega, macizo de Santander, Colombia: evidencias de la orogenia famatiniana en los Andes del norte. *Andean Geology*, *44*(3), 307-327. https://doi.org/10.5027/andgeov44n3-a04

Goldsmith, R., Marvin, R. F., & Maner, H. H. (1971). *Radiometric ages in the Santander Massif, Eastern Cordillera, Colombian Andes.* U.S. Geological Survey Professional Paper 750-D, D44-D49.

Hastie, A. R., Kerr, A. C., Pearce, J. A., & Mitchell, S. F. (2007). Classification of altered volcanic island arc rocks using immobile trace elements: development of the Th Co discrimination diagram. *Journal of Petrology*, *48*(12), 2341-2357. https://doi.org/10.1093/petrology/egm062

Hellstrom, J., Paton, C., Woodhead, J. D., & Hergt, J. M. (2008). Iolite: Software for spatially resolved LA- (quad and MC) ICP-MS analysis. In P. Sylvester (ed.), *Laser Ablation ICP-MS in the Earth sciences: Current practices and outstanding issues* (pp. 343-348). Mineralogical Association of Canada.

Horton, B. K., Saylor, J. E., Nie, J., Mora, A., Parra, M., Reyes-Harker, A., & Stockli, D. F. (2010). Linking sedimentation in the northern Andes to basement configuration, Mesozoic extension, and Cenozoic shortening: evidence from detrital zircon U-Pb ages, Eastern Cordillera, Colombia. *GSA Bulletin*, *122*(9-10), 1423-1442. https://doi.org/10.1130/B30118.1

Huppert, H. E., & Sparks, R. S. J. (1988). The generation of granitic magmas by intrusion of basalt into continental crust. *Journal of Petrology*, *29*, 599-624. https://doi.org/10.1093/petrology/29.3.599

wwJanoušek, V., Farrow, C. M., & Erban, V. (2006). Interpretation of whole-rock geochemical data in igneous geochemistry: Introducing Geochemical Data Toolkit (GCDkit). *Journal of Petrology*, *47*(6), 1255-1259. https://doi.org/10.1093/petrology/egl013

Jeon, H., Williams, I. S., & Chappell, B. W. (2012). Magma to mud to magma: rapid crustal recycling by Permian granite magmatism near the eastern Gondwana margin. *Earth and*

Planetary Science Letters, *319-320*, 104-117. https://doi.org/10.1016/j.epsl.2011.12.010

Jiang, Y. H., Ling, H. F., Jiang, S. Y., Fan, H. H., Shen, W. Z., & Ni, P. (2005). Petrogenesis of a Late Jurassic Peraluminous Volcanic complex and its high-Mg, potassic, quenched enclaves at Xiangshan, Southeast China. *Journal of Petrology*, *46*(6), 1121-1154. https://doi.org/10.1093/petrology/egi012

Leal-Mejía, H. (2011). *Phanerozoic gold metallogeny in the Colombian Andes: A tectono-magmatic approach* [Ph.D. Thesis]. University of Barcelona.

Mantilla, L. C., Bissig, T., Cottle, J. M., & Hart, C. J. (2012). Remains of early Ordovician mantle-derived magmatism in the Santander Massif (Colombian Eastern Cordillera). *Journal of South American Earth Sciences*, *38*, 1-12. https://doi.org/10.1016/j.jsames.2012.03.001

Mantilla, L. C., Bissig, T., Valencia, V., & Hart , C. (2013). The magmatic history of the Vetas-California Mining District, Santander Massif Eastern Cordillera, Colombia. *Journal of South American Earth Sciences*, *45*, 235-249. https://doi.org/10.1016/j.jsames.2013.03.006

Mantilla, L. C., García-Ramírez, C. A., & Valencia, V. A. (2016). Propuesta de escisión de la denominada 'formación Silgará' (macizo de Santander, Colombia), a partir de edades U-Pb en circones detríticos. *Boletín de Geología*, *38*(1), 33-50. https://doi.org/10.18273/revbol.v38n1-2016002

Martens, U., Restrepo, J. J., Ordoñez-Carmona, O., & Correa-Martínez, A. M. (2014). The Tahamí and Anacona terranes of the Colombian Andes: missing links between the South American and Mexican Gondwana margins. *Journal of Geology*, *122*(5), 507-530. https://doi.org/10.1086/677177

McDonough, W. F., & Sun, S. S. (1995). The composition of the earth. *Chemical Geology*, *120*(3-4), 223-253. https://doi.org/10.1016/0009-2541(94)00140-4

Nakamura, N. (1974). Determination of REE, Ba, Fe, Mg, Na and K in carbonaceous and ordinary chondrites. *Geochimica et Cosmochimica Acta*, *38*(5), 757-775. https://doi.org/10.1016/0016-7037(74)90149-5

Ordóñez-Cardona, O., Restrepo Álvarez, J. J., & Pimentel, M. M. (2006). Geochronological and isotopical review of pre-Devonian crustal basement of the Colombian Andes. *Journal of South American Earth Sciences*, *21*(4), 372-382. https://doi.org/10.1016/j.jsames.2006.07.005

Paton, C., Woodhead, J. D., Hellstrom, J. C., Hergt, J. M., Greig, A., & Maas, R. (2010). Improved laser ablation U-Pb zircon geochronology through robust downhole fractionation correction. *Geochemistry, Geophysics, Geosystems*, *11*(3), 1-36. https://doi.org/10.1029/2009GC002618

Peña, M. L., Muñoz Rocha, J. A., & Urueña, C. L. (2018). Laboratorio de Geocronología en el Servicio Geológico Colombiano: avances sobre datación U-Pb en circones mediante la técnica LA-ICP-MS. *Boletín Geológico*, (44), 39-56. https://doi.org/10.32685/0120-1425/boletingeo.44.2018.7

Petrus, J. A., & Kamber, B. S. (2012). VizualAge: A novel approach to laser ablation ICP-MS U-Pb geochronology data reduction. *Geostandards and Geoanalytical Research*, *36*(3), 247-270. https://doi.org/10.1111/j.1751-908X.2012.00158.x

Renne, P. R., Swisher, C. C., Deino, A. L., Karner, D. B., Owens, T. L., & De Paolo, D. J. (1998). Intercalibration of standards, absolute ages and uncertainties in 40Ar/39Ar dating. *Chemical Geology*, *145*(1-2), 117-152. https://doi.org/10.1016/S0009-2541(97)00159-9

Restrepo-Pace, P. (1995). *Late Precambrian to Early Mesozoic Tectonic Evolution of the Colombian Andes based on new geocronological, geochemical and isotopic date* [Ph.D. Thesis]. The University of Arizona.

Restrepo-Pace, P., Ruiz, J., Gehrels, G., & Cosca, M. (1997). Geochronology and Nd isotopic data of Grenville-age rocks in Columbian Andes: new constraints for Late Proterozoice Early Paleozoic paleocontinental reconstructions of Americans. *Earth and Planetary Science Letters*, *150*(3-4), 427-441. https://doi.org/10.1016/S0012-821X(97)00091-5

Restrepo-Pace, P., & Cediel, F. (2010). Northern South America basement tectonics and implications for paleocontinental reconstructions of the Americas. *Journal of South American Earth Sciences*, *29*(4), 764-771. https://doi.org/10.1016/j.jsames.2010.06.002

Ríos, C., García, C., & Takusa, A. (2003). Tectono-metamorphic evolution of the Silgara Formation metamorphic rocks in the Southwestern Santander Massif, Colombian Andes. *Journal of South American Earth Sciences*, *16*(2), 133-154. https://doi.org/10.1016/S0895-9811(03)00025-7

Rodríguez, G., Zapata, G., Correa, A. M., & Arango, M. I. (2017). *Caracterización petrográfica, química y geocronológica del magmatismo Triásico-Jurásico del macizo de Santander-Colombia*. XVI Congreso Colombiano de Geología y III Simposio de Exploradores, Geología, Sociedad y Territorio. Santa Marta, Colombia.

Rodríguez, G., Correa, A. M., Zapata, G., & Arango, M. I. (2017a). *Catálogo Monzogranito de La Corcova, cordillera*

Oriental, departamento de Santander. Servicio Geológico Colombiano.

Rodríguez, G., Correa, A. M., Arango, M. I., Zapata, G., & Bermúdez, J. G. (2020). *Catálogos de las unidades litoestratigráficas de Colombia: Macizo de Santander* (Vol. 1). Servicio Geológico Colombiano. https://doi.org/10.32685/9789585279445

Rodríguez, G., Correa, A. M., Zapata, G., Arango, M. I., Obando-Erazo, G., Zapata-Villada, J. P., & Bermúdez, J. G. (2020a). Diverse Jurassic magmatic arcs of the Colombian Andes: Constraints from petrography, geochronology and geochemistry. In J. Gómez, & A. O. Pinilla Pachón (eds.), *The Geology of Colombia* (vol. 2, pp. 117-170). Publicaciones Geológicas Especiales 36. Servicio Geológico Colombiano. https://doi.org/10.32685/pub.esp.36.2019.04

Rubatto, D. (2002). Zircon trace element geochemistry: Partitioning with garnet and the link between U-Pb ages and metamorphism. *Chemical Geology*, *184*(1-2), 123-138. https://doi.org/10.1016/S0009-2541(01)00355-2

Shand, S. J. (1943). *Eruptive rocks: Their genesis, composition, classification, and their relation to ore-deposits with a chapter on meteorite.* John Wiley & Sons.

Sláma, J., Košler, J., Condon, D. J., Crowley, J. L., Gerdes, A., Hanchar, J. M., Horstwood, M. S. A., Morris, G. A., Nasdala, L., Norberg, N., Schaltegger, U., Schoene, B., Tubrett, M. N., & Whitehouse, M. J. (2008). Plešovice zircon - A new natural reference material for U–Pb and Hf isotopic microanalysis. *Chemical Geology*, *249*(1-2), 1-35. https://doi.org/10.1016/j.chemgeo.2007.11.005

Solari, L., Gómez Tuena, A., Bernal, J., Pérez Arvizu, O., & Tanner, M. (2010). U-Pb zircon geochronology with an integrated LA-ICP-MS microanalytical workstation: Achievements in precision and accuracy. *Geostandards and Geoanalytical Research*, *34*(1), 5-18. https://doi.org/10.1111/j.1751-908X.2009.00027.x

Stacey, J. S., & Kramers, J. D. (1975). Approximation of terrestrial lead isotope evolution by a two-stage model. *Earth and Planetary Science Letters*, *26*(2), 207-221. https://doi.org/10.1016/0012-821X(75)90088-6

Schmid, R., Fettes, D., Harte, B. N., Davis, E. A., Desmons, J. (2007). How to name a metamorphic rock. Recommendations by the IUGS Subcommission on the Systematics of Metamorphic Rocks: Web version 01/02/07. http://www.bgs.ac.uk/SCMR

Streckeisen, A. (1978). IUGS Subcommission on the Systematics of Igneous Rocks: Classification and nomenclature of volcanic rocks, lamprophyres, carbonatites and melilitic rocks; recommendation and suggestions. *Neues Jahrbuch für Mineralogie - Abhandlungen*, *134*, 1-14.

Tang, M., Rudnick, R., McDonough W., Gaschnig R., & Huang, Y. (2015). Europium anomalies constrain the mass of recycled lower continental crust. *Geology*, *43*(8), 703-706. https://doi.org/10.1130/G36641.1

Taylor, S. R., & McLennan, S. M. (1995). The geochemical evolution of the continental crust. *Reviews of Geophysics*, *33*(2), 241-265. https://doi.org/10.1029/95RG00262

Tazzo, D., Weber, B., González-Guzmán, R., Valencia, V., Frei, D., Schaaf, P., & Solari, L. (2018). Multiple metamorphic events in the Palaeozoic Mérida Andes basement, Venezuela: insights from U-Pb geochronology and Hf-Nd isotope systematics. *International Geology Review*, *61*(13), 1557-1593. https://doi.org/10.1080/00206814.2018.1522520

Ulloa, C., & Rodríguez, G. I. (1982). *Intrusivos ácidos Ordovícicos y post – Devónicos en la Floresta (Boyacá)*. VI Congreso Colombiano de Geología, Cali.

Ulloa, C., Guerra, A., & Escovar, R. (1998). *Geología de la Plancha 172 Paz de Río. Escala 1:100.000* [Map]. Ingeominas.

Van der Lelij, R. (2013). *Reconstructing North-Western Gondwana with implications for the evolution of the Iapetus and Rheic Oceans: A geochronological, thermochronological and geochemical study* [Ph.D. Thesis]. Université de Genève.

Van der Lelij, R., Spikings, R., Ulianov, A., Chiaradia, M., & Mora, A. (2016). Palaeozoic to Early Jurassic history of the Northwestern corner of Gondwana, and implications for the evolution of the Iapetus, Rheic and Pacific Oceans. *Gondwana Research*, *31*, 271-294. https://doi.org/10.1016/j.gr.2015.01.011

Vargas, R., Arias, A., Jaramillo, L., & Téllez, N. (1976). *Geología de la plancha 136, Málaga. Escala: 1:100.000* [Map]. Ingeominas.

Vargas, R, Arias, A., Jaramillo, L., & Téllez, N. (1981). *Geología de las planchas 136-Málaga y 152-Soatá, cuadrángulo I-13. Escala 1:100.000. Boletín Geológico*, *24*(3).

Vargas, R., Arias, A., Jaramillo, L., & Téllez, N. (1987). *Geología de la Planchas 152 Soatá. Escala 1:100.000* [Map, version 2009]. Ingeominas.

Ward, D. E., Goldsmith, R., Jimeno, A., Cruz, J., Restrepo, H., & Gómez, E. (1973). *Cuadrángulo H-12, Bucaramanga. Planchas 109, Rionegro, y 120, Bucaramanga. Cuadrángulo H-13, Pamplona. Planchas 110, Pamplona, y 121, Cerrito. Escala 1:100.000. Boletín Geológico*, *21*(1-3).

Watson, E. B., & Harrison, T. M. (1983). Zircon saturation revisited: temperature and composition effects in a variety of crustal magma types. *Earth and Planetary Science Letters*, *64*(2), 295-304. https://doi.org/10.1016/0012-821X(83)90211-X

Wiedenbeck, M., Allé, P., Corfu, F., Griffin, W. L., Meier, M., Oberli, F., Von Quadt, A., Roddick, J. C., & Spiegel, W. (1995). Three natural zircon standards for U-Th-Pb, Lu-Hf, trace element and REE analyses. *Geostandards Newsletter*, *19*(1), 1-23. https://doi.org/10.1111/j.1751-908X.1995.tb00147.x

Wiedenbeck, M., Hanchar, J. M., Peck, W. H., Sylvester, P., Valley, J., Whitehouse, M., & Zheng, Y. F. (2004). Further characterisation of the 91500 zircon crystal. *Geostandards and Geoanalytical Research*, *28*(1), 9-39. https://doi.org/10.1111/j.1751-908X.2004.tb01041.x

Winchester, J. A., & Floyd, P. A. (1977). Geochemical discrimination of different magma series and their differentiation products using immobile elements. *Chemical Geology*, *20*, 325-343. https://doi.org/10.1016/0009-2541(77)90057-2

Zapata, G. Correa, A. M., Rodríguez, G., & Arango, M. I. (2017). *Monzogranito de Santa Rosita, cordillera Oriental, departamentos de Santander y Boyacá*. Servicio Geológico Colombiano.

Zuluaga, C. A., Amaya S., Urueña, C., & Bernet, M. (2017). Migmatization and low-pressure overprinting metamorphism as record of two pre-Cretaceous tectonic episodes in the Santander Massif of the Andean basement in northern Colombia (NW South America). *Lithos*, *274-275*, 123-146. https://doi.org/10.1016/j.lithos.2016.12.036